J. Marine Sci. Appl. (2015) 14: 61-68
DOI: 10.1007/s11804-015-1295-9

Numerical Investigations on the Aerodynamic Performance of Wind Turbine: Downwind Versus Upwind Configuration

Hu Zhou[1,3] and Decheng Wan[1,2*]

1. State Key Laboratory of Ocean Engineering, School of Naval Architecture, Ocean and Civil Engineering, Shanghai Jiao Tong University, Shanghai 200240, China
2. Collaborative Innovation Center of Advanced Ship and Deep-Sea Exploration, Shanghai 200240, China
3. Power China Huadong Engineering Corporation Limited, Hangzhou 310014, China

Abstract: Although the upwind configuration is more popular in the field of wind energy, the downwind one is a promising type for the offshore wind energy due to its special advantages. Different configurations have different aerodynamic performance and it is important to predict the performance of both downwind and upwind configurations accurately for designing and developing more reliable wind turbines. In this paper, a numerical investigation on the aerodynamic performance of National Renewable Energy Laboratory (NREL) phase VI wind turbine in downwind and upwind configurations is presented. The open source toolbox OpenFOAM coupled with arbitrary mesh interface (AMI) method is applied to tackle rotating problems of wind turbines. Two 3D numerical models of NREL phase VI wind turbine with downwind and upwind configurations under four typical working conditions of incoming wind velocities are set up for the study of different unsteady characteristics of the downwind and upwind configurations, respectively. Numerical results of wake vortex structure, time histories of thrust, pressure distribution on the blade and limiting streamlines which can be used to identify points of separation in a 3D flow are presented. It can be concluded that thrust reduction due to blade-tower interaction is small for upwind wind turbines but relatively large for downwind wind turbines and attention should be paid to the vibration at a certain frequency induced by the cyclic reduction for both configurations. The results and conclusions are helpful to analyze the different aerodynamic performance of wind turbines between downwind and upwind configurations, providing useful references for practical design of wind turbine.

Keywords: offshore wind energy; wind turbine; downwind and upwind configuration; wake flows; arbitrary mesh interface (AMI); OpenFOAM; aerodynamic performance

Article ID: 1671-9433(2015)01-0061-08

1 Introduction

With traditional energy rapidly depleting and global climate deteriorating, renewable energy, especially wind energy, is becoming increasingly concerning (Wu *et al.*, 2014; Hong and Moller, 2012). There are two types of common configurations for wind turbines: upwind and downwind. Although the upwind type is more popular than the other one, the advantage that the downwind configuration can face the wind automatically makes them more promising for offshore wind turbines. Therefore, it is important to predict the aerodynamic performance of both downwind and upwind configurations accurately for designing and developing more reliable wind turbines.

With the development of computer hardware technology and numerical methods, the computational fluid dynamics (CFD) has been increasingly used to analyze the aerodynamic performance of the wind turbines. Duque *et al*. (1999) carried out a Navier-Stokes simulation of a downwind three-bladed wind turbine with overset grids strategy to examine the rotor-tower interaction. Janajreh *et al*. (2010a) presented a 2D numerical simulation of a downwind turbine to investigate the interaction between tower wake and blade. The 5%, 17% and 57% reductions of the aerodynamic lift forces were observed separately. Janajreh *et al*. (2010b) also made a quantitative analysis on the blade-tower interaction to quantify the resulting drag coefficients on a moving downwind turbine blade. It should be noted that the governing equations were first setup in an Arbitrary Lagrangian/Eulerian frame. Zahle *et al*. (2009) used an in-house code called EllipSys3D to compare the aerodynamic performance of an isolated rotor and a downwind wind turbine. The unsteady interactions between the tower wake and rotor blades were successfully captured. As to upwind wind turbines, since the rotor is placed on the upstream side of the tower, the interference effect is not pronounced when compared with downwind configurations, relevant studies are in a small amount. Li *et al*. (2012) studied the NREL phase VI wind turbine using CFDShip-Iowa v4.5 to investigate the aerodynamic performance of the blades and their results showed satisfactory agreement with experimental results. Wang *et al*. (2012) studied the blade-tower interaction using OpenFOAM. The conclusion showed that the blade-tower interactions had little effect on the whole aerodynamic

Received date: 2014-06-30.
Accepted date: 2014-11-09.
Foundation item: Supported by the National Natural Science Foundation of China (Grant Nos. 51379125, 51411130131, 11432009), the National Key Basic Research Development Plan (973 Plan) Project of China (Grant No. 2013CB036103), High Technology of Marine Research Project of the Ministry of Industry and Information Technology of China, ABS(China), and the Program for Professor of Special Appointment (Eastern Scholar) at Shanghai Institutions of Higher Learning (Grant No. 2013022).
***Corresponding author Email:** dcwan@sjtu.edu.cn

performance of an upwind wind turbine.

Most literatures give the aerodynamic performance of wind turbines with a single configuration, and until now numerical solutions by CFD to compare the dynamic response between upwind and downwind configurations in details are still quite scarce. In this paper, a CFD method based on the open source toolbox OpenFOAM coupled with arbitrary mesh interface (AMI) method (Wang *et al*, 2012; Zhao and Wan, 2014) is introduced to study the aerodynamic performance of wind turbines, especially the wake shedding from the rotor, and the interaction between the tower wake and rotor blades. The essence of AMI method is a kind of sliding mesh, and the algorithm behind it is described in the paper written by Farrell and Maddison (2011). The AMI method is a special technique that allows simulation across disconnected, adjacent mesh domains which can move relatively to one another.

The paper will be organized as follows: Firstly, the numerical method of OpenFOAM coupled with AMI method is presented. Then, the computational details, including the description of the wind turbine model, mesh strategy and discretization schemes are given. Furthermore, results and discussion about the analysis and comparisons are presented. Finally, the conclusions are drawn.

2 Numerical method

In this paper, all our cases are computed by PimpleDyMFoam solver based on OpenFOAM, which is an open source CFD 'library' written with object-oriented design to solve problems of computational continuum mechanics. It offers a flexible set of efficient libraries, utilities and solvers, based on which everyone can revise and redesign their own solvers according to specific problems. PimpleDyMFoam is a transient solver for incompressible flow of Newtonian fluids. Although there are no experimental data available in terms of the work in this paper, the solver used has been validated for predictions of the aerodynamic performance of wind turbines by Wang *et al*. (2012), Zhao *et al*. (2014), Zhao and Wan (2014).

Due to low wind velocity around the wind turbine (Ma < 0.3), the flow can be considered as incompressible. Since the density of air is very small, the gravity is neglected. Using the time-averaging technology, the governing equations can be written as:

$$\frac{\partial U_i}{\partial x_i}=0 \tag{1}$$

$$\frac{\partial U_i}{\partial t}+\frac{\partial}{\partial x_j}(U_iU_j)=-\frac{1}{\rho}\frac{\partial P}{\partial x_i}+\frac{\partial}{\partial x_j}\left(\nu\frac{\partial U_i}{\partial x_j}-\overline{u_i'u_j'}\right) \tag{2}$$

Eq. (1) is the continuity equation derived from mass conservation, and Eq. (2) is the momentum equation in the viewpoint of Newton's second law. Where U_i and P are the time-averaged velocity and pressure respectively and ν is kinematic viscosity. A new term $\frac{\partial}{\partial x_j}\left(\overline{u_i'u_j'}\right)$ called Reynolds stress appears in Eq. (2), which represents the relationship between the fluctuating velocities.

In order to solve the equations, the Reynolds stress term must be modeled by turbulence model. The most common two-equation model *k*-*ω*SST is chosen to get close to the equations. The model behaves like *k*-*ω* turbulence model in the regions close to the wall and like the standard *k*-*ε* turbulence model in free-stream regions. The *k*-*ω*SST turbulence model is very suitable for simulating the aerodynamic performance of wind turbines because of its good behavior in adverse pressure gradients and separating flow. For the details of *k*-*ω*SST turbulence model, refer to related papers (Menter, 1994; 2009).

AMI was used as a boundary condition for the patches between the two domains to allow simulation between them (Zhao and Wan, 2014; Zhou and Wan, 2014). The principle behind AMI is to project the interface patch of one domain onto that of the other domain and interpolate. Its implementation can be divided into four steps. The first one is to define the AMI interface (sliding interface) that would separate rotor and stator part of the whole mesh domain, which can be done by using the creatAMIFaces and createBafflesDict utilities in OpenFOAM. Then, a search algorithm is set to find the neighbouring cells between the interfaces. The third step is to calculate the weighting factor based on the overlapping area of adjacent cells. Finally, a set of weighting factors calculated in the previous step can be used to balance the mass and momentum flux at the AMI interface. The AMI is integrated into boundary patch classes in OpenFOAM and is available for the computation of rotating machinery. The mesh required special treatments for the AMI region, and for the details of the mesh, refer to the following of mesh strategy.

3 Computational details

3.1 Wind turbine model description

The NREL Phase VI wind turbine is an important benchmark model for numerical simulation to validate their computational methods. The blade is tapered and twisted with the NREL S809 profile, the relationship between the local twist angle and the normalized rotor radius is shown in Fig. 1. It should be noted that our cone angle is 0 which may be different from the experiment. Because the real rotor is flexible, the cone angle is close to 0 when rotating. Assuming the cone angel to be 0, the effect of yaw of wind turbine is not considered either for convenience. The basic geometric parameters of the wind turbine are organized in following table (Hand *et al*., 2001).

The computational model is set up by CATIA. The upwind and downwind configurations of the geometric model can be shown in subsequent figures (Fig. 4). In order to assess the blade-tower interaction, the distance from yaw-axis to teeter pin stays the same, which is 1.469 m.

Table 1 Geometric parameters of model

Geometric model	Values
Numbers of blades	2
Diameter of rotor/m	10.058
Rotational speed/(r·min^{-1})	72
Location of rotor	Upwind Downwind
Hub height/m	12.192
Pitch angle/(°)	3

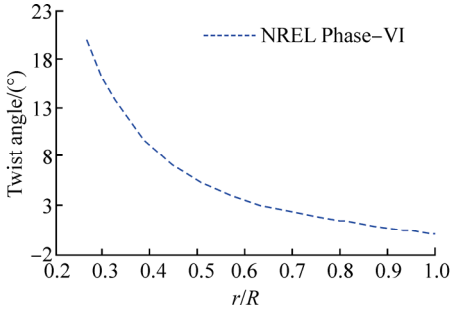

Fig. 1 Local twist angle along the blade

3.2 Mesh strategy

The mesh generation used in OpenFOAM has a big difference with other general software, like Gambit, Pointwise and so on. In OpenFOAM, only the background mesh and the 3D model are needed. In this project, two steps are considered to build mesh: project predefined background mesh onto the surface and then split hexahedral-cells from STL surface (wind turbine model). These can be carried out easily by the powerful utility called snappyHexMesh in OpenFOAM. The predefined background mesh is established by ANSYS ICEM-CFD. In order to get mesh with good quality, the cell aspect ratio of predefined background mesh around the wind turbine should be approximately 1.

Although there are two different computational models, the mesh strategy is the same. An inner side of O-type block is used to ensure the mesh quality of the AMI faces, and the mesh cell surrounded by the AMI faces will be marked to rotate with the wind turbine at the same rotational speed. The flow field information between rotating mesh and static mesh exchanges at the AMI faces through interpolation. In the end, the numbers of cells of two different models are almost the same, about 60 000. The refinement of mesh is set up according to the distance to the object in OpenFOAM, that's to say, the closer to the object, the denser of the grid. The y+ is around 50. As for the mesh quantity, balance must be made between the computational efficiency and the computational accuracy. The upstream inlet is located at 5 m ahead of the wind turbine and the downstream outlet is located at 20 m behind the wind turbine. This setup is based on other researchers' work—the computational efficiency and accuracy. The global mesh, the mesh of AMI region of downwind and upwind wind turbines are shown in Fig. 2 and Fig. 3, respectively.

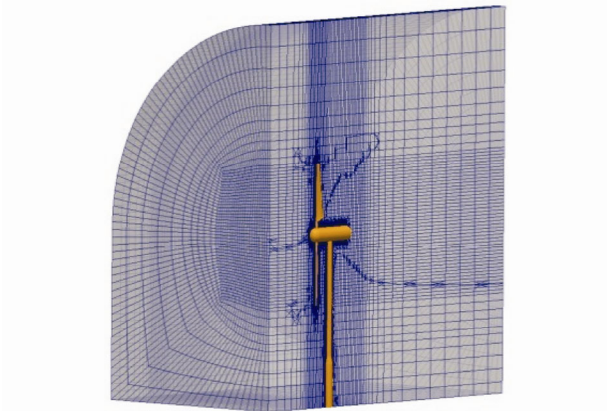

Fig. 2 Global mesh overview

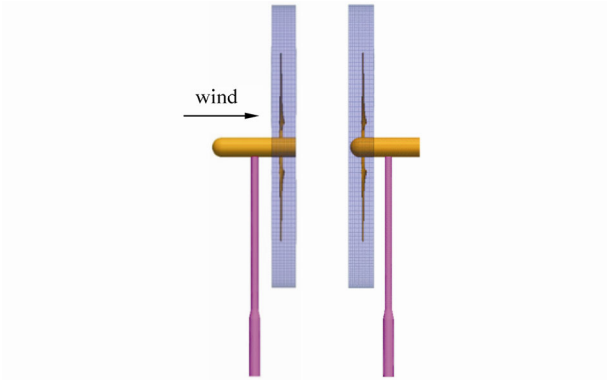

Fig. 3 AMI region of downwind and upwind configurations

3.3 Discretization schemes

The finite volume method (FVM) is used to solve governing equations in any unstructured mesh consisting of polyhedral cells. In OpenFOAM, the dependent variable and other parameters are stored at cell centers. The interpolation from cell centers to face centers is done by linear scheme. The first and second time derivatives are discretized with a second-order Euler implicit scheme. The convective term is set to 'Gauss linearUpwind' scheme in which Gauss keyword stands for 'finite volume discretization' and linear scheme is the most effective option. The discretization of diffusion terms is done in 'Gauss linear correct' scheme where 'correct' means an additional correction term will be added on the non-orthogonal mesh to preserve second order accuracy (Jasak, 1996). The pressure-velocity treatment is decoupled by PIMPLE algorithm—a blended algorithm that combines SIMPLE (Semi-implicit Method for Pressure-Linked Equation) algorithm (Patankar, 1980) and PISO (Pressure Implicit with Splitting of Operators) algorithm (Issa, 1986).

3.4 Other details

The case requires initial and boundary conditions settings for all the involved fields. For the velocity, the inlet patch is set to a constant value, which equals to the wind velocity, and the others are set to the zero gradient. For the pressure, the inlet patch is set to zero gradient while the outlet patch is set to zero, which is only a reference point.

The computational time step in this case is determined according to maximum courant number during the simulation. According to the stability and convergence of the results, the total revolution being simulated is about 3 rounds.

4 Computational results

4.1 Wake vortex structure

As the wind passes through the wind turbine, a wake or disturbed, turbulent region is created behind it. The wake influences not only the aerodynamic performance of the turbine that produces it, but also the wind turbines located in it (Kim *et al.*, 2015; Jadhav and Roy, 2014). So the wake vortex structure is an important part in aerodynamic performance research. In present study, the wake vortex structure is visualized by the contour of the second invariant of the velocity gradient tensor Q. Different Q is used at different wind speed. The value of Q is determined based on the clarity of visualization. For the wind speed of 5 m/s, Q is 1.4, and for the wind speed of 10 m/s, Q is 5. It should be noted that the legend had been changed when plotting the picture for the sake of clarity of visualization, so the value in the plot is meaningless. The definition of Q is in the following equation:

$$Q=\frac{1}{2}(\Omega_{ij}\times\Omega_{ij}-S_{ij}\times S_{ij}) \tag{3}$$

where $\Omega_{ij}=\frac{1}{2}(u_{i,j}+u_{j,i})$, $S_{ij}=\frac{1}{2}(u_{i,j}-u_{j,i})$. So Q represents the local balance between shear strain rate and vortices magnitude (Jeong and Hussain, 1995).

The vortex structures for downwind and upwind configurations at 5 m/s and 10 m/s are shown in Fig. 4. Whatever the configuration is, distinct blade tip vortices and root vortices are observed. The existence of vortices will lead to sharp gradients in the velocity and peaks in the turbulence intensity (Sanderse *et al.*, 2011).

For 5 m/s, careful comparison of the blade tip vortices between upwind and downwind shows some key differences. The blade tip vortices of the downwind turbine are much smoother, while those of upwind turbine cut by the tower can be viewed clearly. Additionally, since the geometry of the blade changes quickly from a cylinder to S809 profile, the root vortices can also be observed evidently and the interaction between root vortices and tower is also obvious for the upwind turbine. Briefly speaking, the configurations of wind turbine have a significant impact on the interaction between tower and tip vortices or root vortices.

When it comes to 10 m/s, dynamic stall phenomena may occur partly on blades. Even for the downwind configuration, the interaction between vortices and tower is also distinct in Fig. 4. However, the interaction of upwind wind turbines is more serious and the wake structures behind it are very disordered.

It also should be noted that the wake shedding and the interaction between blade and tower can be surveyed and compared distinctly, and almost all the vortical structures dissipate fast after moving about one blade length due to the coarse mesh. Therefore, in order to study the wake structure far away from the turbine, a longer region of refined mesh or vorticity confinement method (Steinhoff, 1994) without increasing the grid size are necessary. In this paper, due to the limited computer resources, the mesh is not fine enough, so it may cause some unphysical phenomenal especially for the downwind configurations (Moshfeghi *et al.*, 2012).

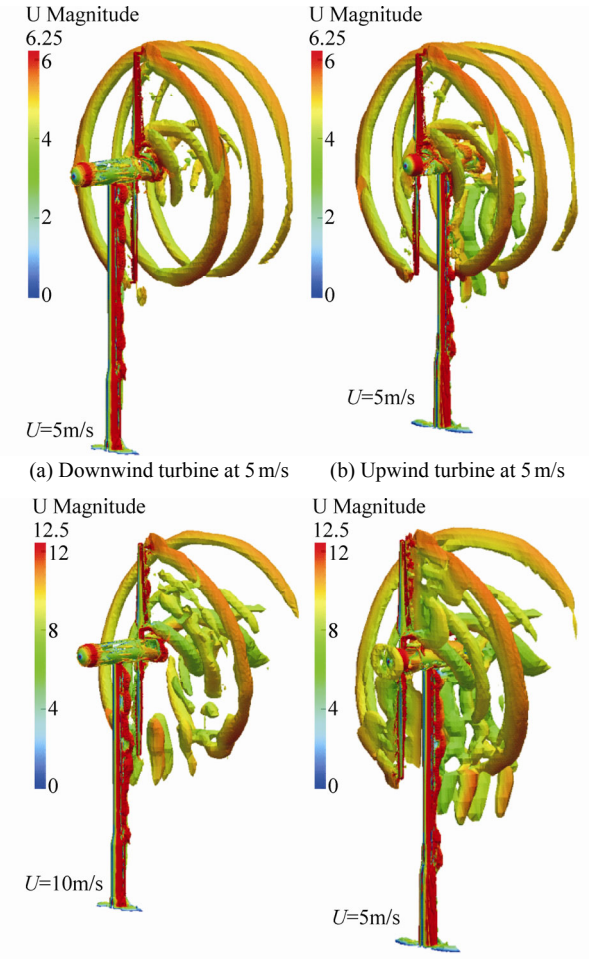

(a) Downwind turbine at 5 m/s (b) Upwind turbine at 5 m/s

(c) Downwind turbine at 10 m/s (d) Upwind turbine at 10 m/s

Fig. 4 Instantaneous vortex structure for downwind and upwind at 5 and 10 m/s

4.2 Time histories of thrust

Fig. 5 shows the time histories of thrust at 5, 10, 15, and 25 m/s for different configurations. It should be noted that the thrust here is achieved by pressure integral of only one blade surface. The azimuth angle is zero when the rotor is upward and parallel to the tower. The big difference between upwind and downwind configurations is that the downwind configuration thrust will drop sharply and rapidly when the azimuthal angle passes 180 degrees. The thrust of the upwind wind turbine suffers a drop in comparison with the rotor-only model when the blade passes through the tower but the reduction of thrust only accounts for a small percentage (Wang *et al.*, 2012). The situation is not the same

when concerning the difference between upwind and downwind configurations. For the upwind configuration, the drop of thrust is less than 10% of the mean thrust. However, for the downwind configuration, the amplitude of the steep fall accounts for about 35%. The percentage even reaches 38.4% at a wind speed of 10 m/s.

Another interesting phenomenon which should be noted is that the thrust will exceed the mean value and form a peak when the azimuthal angle is between 180 and 240 degrees. This phenomenon is quite evident especially when the wind speed is 10 m/s and 15 m/s. The reasons are complicated and several-fold. Suppose that this may be caused by the impacts of wake of the tower, but it needs to be validated deeply in the next step.

Therefore, it can be concluded that thrust reduction due to blade-tower interaction is small for upwind wind turbines but is relatively large for downwind wind turbines. To both configurations, attention should be paid to the vibration at a certain frequency induced by the cyclic reduction.

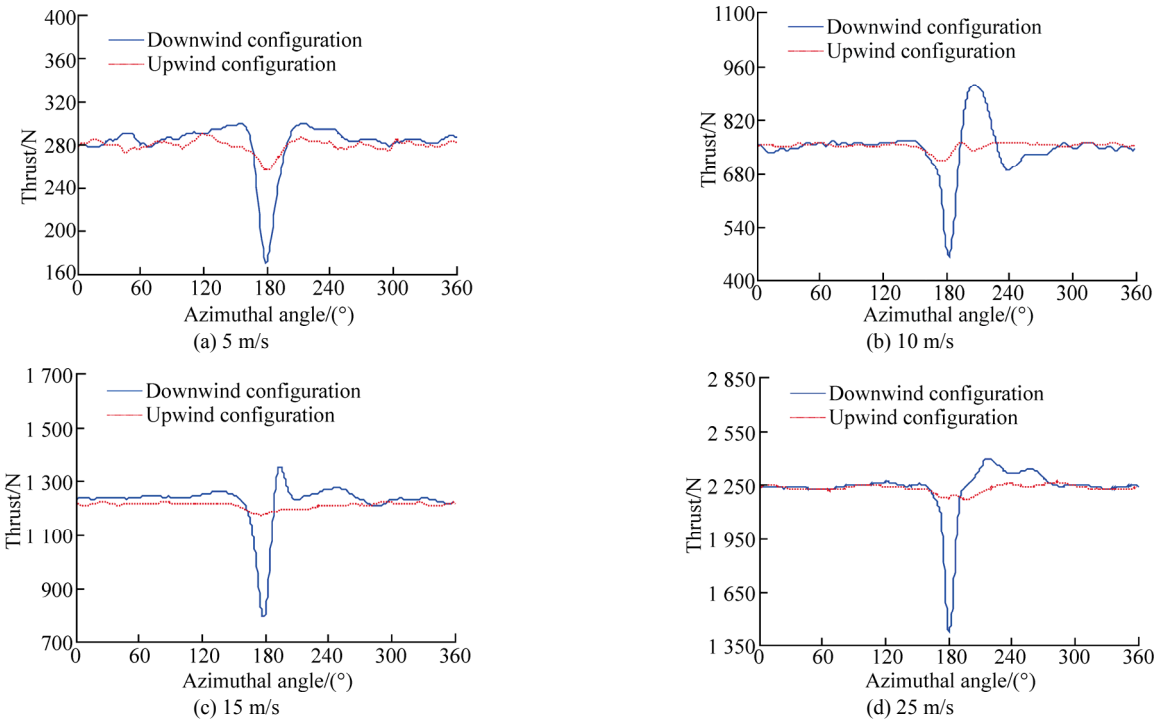

Fig. 5 Time histories of thrust for different wind speeds

4.3 Limiting streamlines

To the computation of the viscous incompressible flows, the velocity on a solid surface is zero. So, streamlines cannot be defined directly on a solid surface. But when coordinates normal to the surface approach 0 as a limit, the streamline exists and it is called limiting streamline. In this paper, the limiting streamline is drawn through skin friction lines which are used to identify points of separation in a 3D flow.

As can be seen from Figs. 6 and 7, the limiting streamlines on the pressure side of the blade are almost identical to 5 m/s. The direction x points from the leading edge to the trailing edge and the Chord is the length between leading point and trailing point. It can be observed that on the suction side for both configurations, starting from roughly x/Chord=0.5, streamlines deviate from the parallel inboard streamlines towards the spanwise direction, which may be caused by the centrifugal acceleration induced by rotation. The two configurations show some differences on the suction side. Firstly, the spanwise flow movement closest to the root for the upwind configuration is more evident than that of the downwind configuration. Additionally, the points of flow separation are different.

For 10 m/s, there are a few differences in the limiting streamlines on the pressure side closest to tip and the other places seem to be the same. Figs. 7(b) and 7(d) shows that the spanwise movements occupy most of the suction side of the blade. The part closest to blade tip for both configurations have a subtle distinction, because the blade has stalled partly at a wind speed of 10 m/s and the tower impact is very different.

4.4 Pressure distributions

Pressure distributions for three spanwise sections are compared at r/R=0.3, 0.63 and 0.95 (Figs. 8 and 9). The pressure distribution is calculated at an azimuthal angle of 180 degrees and the definition of it is in the following:

$$C_p = \frac{P_\infty - P_0}{\frac{1}{2}\rho C\left(W_\infty^2 + (r\omega)^2\right)} \tag{4}$$

The normalization of the pressure coefficient is adopted by the National Renewable Energy Laboratory (NREL). In prior related published papers, the pressure coefficient defined before is used to compare the numerical results with

experiment results provided by Sherer and Scott (2005). For the continuity of this research, the same definition of pressure coefficient is used.

For the lower computed wind speed of 5 m/s, the figures show some deviation of pressure distributions for the two configurations. Two trends are observed in Fig. 8. One is that the deviations at the leading edge are much larger when compared with the trailing edge. The other one is that the deviations at root are the largest and when the section moves to the tip, the deviations become less and less.

For wind speed of 10 m/s, the two trends are still valid. In addition, a leading edge separation at the r/R=0.3 section for the downwind configuration is seen and the configuration preserves a sharp suction peak. But the upwind configuration has a less pronounced suction peak. The great difference in the pressure distributions can lead to the great difference in the thrust which can be seen from the time histories of thrust analysis.

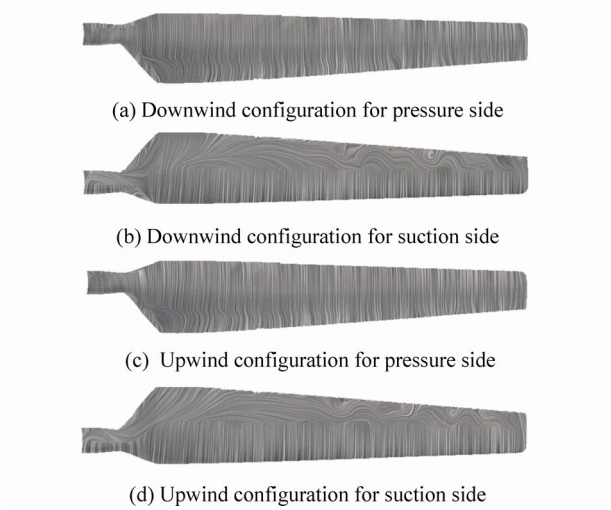

Fig. 6 Instantaneous limiting streamline at 5 m/s for both configurations

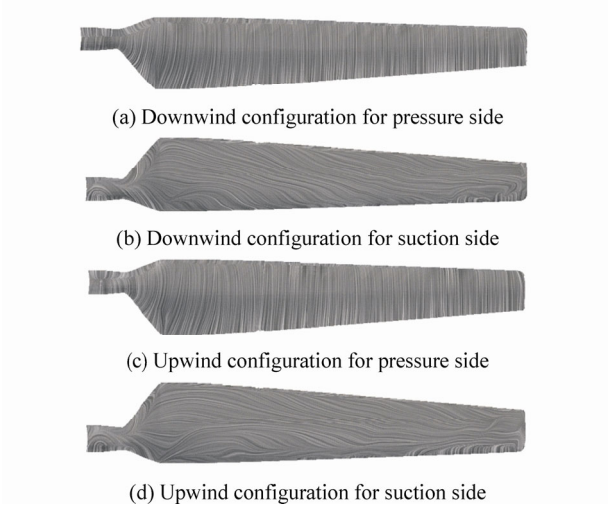

Fig. 7 Instantaneous limiting streamline at 10 m/s for both configurations

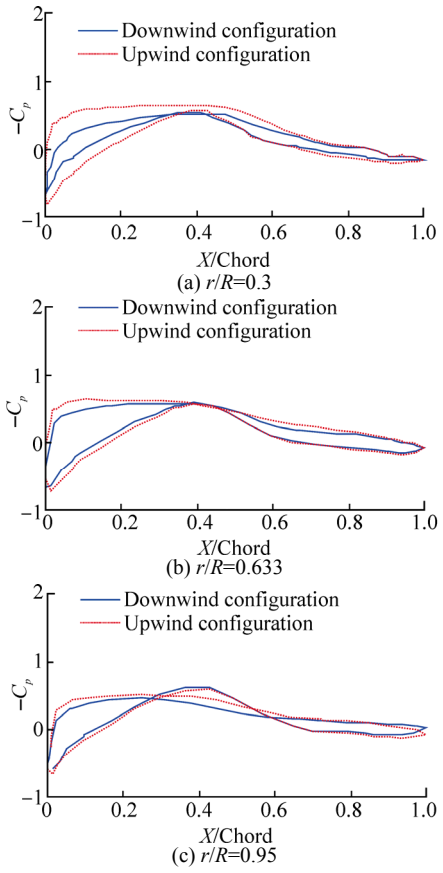

Fig. 8 Pressure coefficient distribution at 5 m/s sections

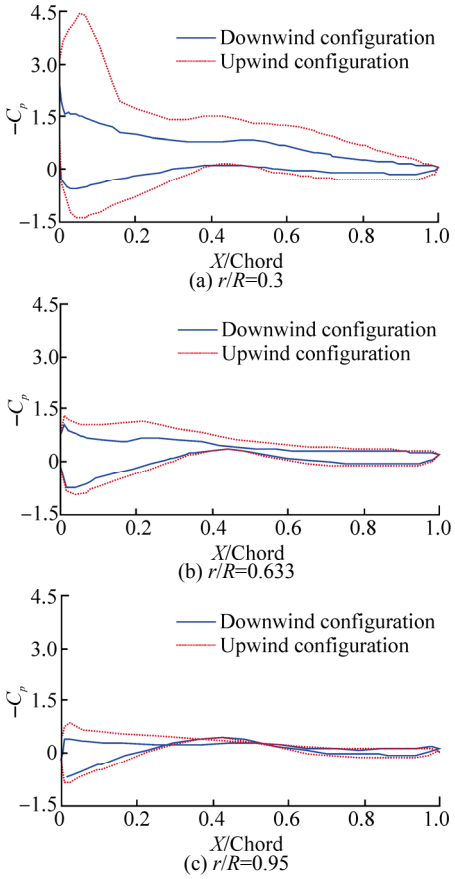

Fig. 9 Pressure coefficient distribution at 10 m/s sections

5 Conclusions

Numerical solutions of the aerodynamic performance of wind turbines: downwind versus upwind configurations are obtained by using open source OpenFOAM unsteady RANS solver coupled with AMI method to handle mesh movements. The NREL phase VI wind turbines in both downwind and upwind configurations are chosen for numerical tests with different incoming wind speeds (5 m/s and 10 m/s) at a fixed blade pitch. Detailed numerical results of wake vortex structure, time histories of thrust and pressure distribution on the blade and limiting streamlines are illustrated and analyzed. It has been found that the configuration of wind turbine has a significant impact on the interaction between tower and tip vortices or root vortices which can be clearly seen from the wake vortex structure and limiting streamline. When the thrust descends less than 10% of the mean thrust for the upwind configuration, the amplitude falls about 35% of the mean thrust for the downwind configuration, so the vibration at a certain frequency induced by the cyclic reduction should be noticed. Since the deviations of pressure distribution at the leading edge are much larger than those at the trailing edge, it can be obtained that the deviations become less and less with the section moving to the tip. In order to provide a more accurate numerical model for practical application, the random wind and the multiphase flow in offshore wind turbines should be considered. These problems may be solved in future studies. The results obtained are meaningful and applicable for further research in the field of wind turbines.

References

Duque, EPN, Van Dam CP, Brodeur RR, Chao DD (1999). Navier-Stokes analysis of time-dependent flows about wind turbines. *Proceedings of the 1999 3rd ASME/JSME Joint Fluids Engineering Conference*, San Francisco, USA, 1-6.

Farrell P, Maddison J (2011). Conservative interpolation between volume meshes by local Galerkin projection. *Computer Methods in Applied Mechanics and Engineering*, **200**(1), 89-100.
DOI: 10.1016/j.cma.2010.07.015

Hand MM, Simms DA, Fingersh LJ, Jager DW, Cotrell JR, Schreck S, Larwood SM (2001). *Unsteady aerodynamics experiment phase VI: Wind tunnel test configuration and available data campaigns*. National Renewable Energy Laboratory, Golden, Colorado, USA, NREL/TP-500-29955.
DOI: 10.2172/787980

Hong LX, Moller B (2012). Feasibility study of China's offshore wind target by 2020. *Energy*, **48**(1), 268-277.
DOI: 10.1016/j.energy.2012.03.016

Issa RI (1986). Solution of the implicitly discretised fluid flow equations by operator-splitting. *Journal of Computational physics*, **62**(1), 40-65.
DOI: 10.1016/0021-9991(91)90191-M

Jadhav HT, Roy R (2014). Effect of turbine wake on optimal generation schedule and transmission losses in wind integrated power system. *Sustainable Energy Technologies and Assessments*, **7**, 123-135.
DOI: 10.1016/j.seta.2014.04.001

Janajreh I, Talab I, Macpherson J (2010a). Numerical simulation of tower rotor interaction for downwind wind turbine. *Modelling and Simulation in Engineering*, **2010**(10), 23-45.
DOI: 10.1155/2010/860814

Janajreh I, Qudaih R, Talab I, Ghenai C (2010b). Aerodynamic flow simulation of wind turbine: Downwind versus spwind configuration. *Energy Conversion and Management*, **51**(8), 1656-1663.
DOI: 10.1016/j.enconman.2009.12.013

Jasak H (1996). *Error analysis and estimation for the finite volume method with applications to fluid flows*. PhD thesis, Imperial College London, University of London.

Jeong J, Hussain F (1995). On the identification of a vortex. *Journal of Fluid Mechanics*, **285**(69), 69-94.
DOI: http://dx.doi.org/10.1017/S0022112095000462

Kim SH, Shin HK, Joo YC, Kim KH (2015). A study of the wake effects on the wind characteristics and fatigue loads for the turbines in a wind farm. *Renewable Energy*, **74**, 536-543.
DOI: 10.1016/j.renene.2014.08.054

Li Y, Paik KJ, Xing T, Carrica PM (2012). Dynamic overset CFD simulations of wind turbine aerodynamics. *Renewable Energy*, **37**(1), 285-298.
DOI: 10.1016/j.renene.2011.06.029

Menter FR (1994). Two-equation eddy-viscosity turbulence models for engineering applications. *AIAA Journal*, **32**(8), 1598-1605.
DOI: 10.2514/3.12149

Menter FR (2009). Review of the shear-stress transport turbulence model experience from an industrial perspective. *International Journal of Computational Fluid Dynamics*, **23**(4), 305-316.
DOI: 10.1080/10618560902773387

Moshfeghi M, Song Yajun, Xie Yonghui (2012). Effects of near-wall grid spacing on SST-K-ω model using NREL phase VI horizontal axis wind turbine. *Journal of Wind Engineering and Industrial Aerodynamics*, **107-108**, 94-105.
DOI: 10.1016/j.jweia.2012.03.032

Patankar SV (1980). *Numerical heat transfer and fluid flow*. Washington, DC, Hemisphere Publishing Corp., USA.

Sanderse B, Van der Pijl SP, Koren B (2011). Review of computational fluid dynamics for wind turbine wake aerodynamics. *Wind Energy*, **14**(7), 799-819.
DOI: 10.1002/we.458

Sherer SE, Scott JN (2005). High-order compact finite-difference methods on general overset grids. *Journal of Computational Physics*, **210**(2): 459-496.
DOI: 10.1016/j.jcp.2005.04.017

Steinhoff J (1994). Vorticity confinement: A new technique for computing vortex dominated flows. *In:* Caughey DA, Hafez MM (Eds.), *Frontiers of Computational Fluid Dynamics*. Wiley, New York, 235-264.

Wang Q, Zhou H, Wan DC (2012). Numerical simulation of wind turbine blade-tower interaction. *Journal of Marine Science and Application*, **11**(3), 321-327.
DOI: 10.1007/s11804-012-1139-9

Wu Jie, Wang Zhixin, Wang Guoqiang (2014). The key technologies and development of offshore wind farm in China. *Renewable and Sustainable Energy Reviews*, **34**(C), 453-462.
DOI: 10.1016/j.rser.2014.03.023

Zahle F, Sørensen NN, Johansen J (2009). Wind turbine rotor-tower interaction using an incompressible overset grid method. *Wind Energy*, **12**(6), 594-619. DOI: 10.1002/we.327

Zhao WC, Cheng P, Wan DC (2014). Numerical computation of aerodynamic performances of NREL offshore 5-MW baseline wind turbine. *Proceedings of the Eleventh (2014) ISOPE Pacific Asia Offshore Mechanics Symposium*, Shanghai, China, 13-18.

Zhao WC, Wan DC (2014). Wind turbine impacts on its semi-submersible floating supporting system for phase II of OC4. *Proceedings of the Twenty-fourth (2014) International Ocean and Polar Engineering Conference*, Busan, Korea, 294-301.

Zhou H, Wan DC (2014). Numerical simulation of the unsteady flows around wind turbines with different blades numbers. *Chinese Journal of Hydrodynamics*, **29**(4), 444-453. (in Chinese) DOI: 10.3969/j.issn1000-4874.2014.04.009

The 12th International Conference on the Stability of Ships and Ocean Vehicles (STAB 2015)

14th-19th June, 2015, Glasgow, Scotland

As ancient as Archimedes (circa 250 BC), the topic of stability of ships (and more generally of floating bodies) has fascinated eminent scientists throughout the centuries, of the likes of Huygens, Bougue, Euler and the Bernoullis. Despite unrelenting efforts institutionally, country-wide and world scale, the field remains relevant and of high focus, combining deep scientific basis with practical and ethical concerns stemming from a continually changing industry and society.

Stability represents a prime driver for naval architects. It is not a coincidence that the first risk-based approach to ship design used “damage” stability as raw model whilst the form and consequences of “intact” and “damage” stability regulations remain at the forefront of interest at IMO.

For 40 years the STAB conferences and the affiliated workshops are the definitive meeting venues of maritime researchers and professionals who are interested in problems of dynamic stability and safety. All important advances that have taken place during this period in the numerical and physical modelling and understanding of ship stability, advances in extreme vessel dynamics and the development of new stability regulations have been instigated, presented and debated at some STAB meeting.

The forthcoming STAB will be organised by the University of Strathclyde in Scotland, UK. Established in 1796 as the ‘place of useful learning’ it is today Scotland’s third largest university with an international reputation and outlook and with students and staff from over 100 countries. The Department of Naval Architecture, Ocean and Marine Engineering (NAOME), is one of the largest in Europe and worldwide. With an illustrious history stretching back to 1882 and the host of John Elder Chair, the first in Naval Architecture, NAOME is a key provider of Marine Technology expertise in the marine and offshore sectors

Researchers, professionals and all interested to fathom stability of ships and ocean vehicles, from theory to practical implementation, are warmly invited to participate in STAB 2015 in Glasgow and actively contribute to furthering and to disseminating knowledge in this critical field of maritime safety.

Please visit the STAB Conference web site www.stab2015.org at regular.

Conference Topics

Technical papers are invited addressing the following themes:

- Ship dynamic stability in rough seas
- Damage stability of passenger and cargo ships
- Probabilistic and risk-based assessment of stability
- Nonlinear dynamics of extreme ship behaviour
- Modes of ship capsize and design to improve stability
- Second generation intact stability criteria
- The implication of stability regulations for design
- Ship stability accident investigation
- Stability of high-speed craft
- Fishing vessel safety
- Naval ship stability
- Stability of floating platforms
- Stability of offshore supply vessels
- Unconventional problems of stability
- Dynamic instability other than in roll motion
- Modeling of environmental excitations
- Risk-Based Intact-Damage stability integration
- Decision support and operational guidance in normal operation and in emergencies
- Operation in polar waters and ice

Topics of special local interest:

- Capsize due to cargo liquefaction
- Stability of Tankers and FPSOs
- Stability of old ships – passenger and cargo